Original Article

Evaluation of low-dose chest scans for coronary artery calcium scoring using photon-counting computed tomography with different slice thicknesses and iterative reconstruction levels

Yan-E Zhao[1#^], Qiuju Hu[1#], Jiajia Zhu[1], Huixin Zhang[1], Jiliang Chen[2], Meirong Sun[1], Dongsheng Jin[1], Guangming Lu[3], Song Luo[1]

[1]Department of Radiology, Geriatric Hospital of Nanjing Medical University, Nanjing, China; [2]Siemens Healthineers CT Collaboration, Shanghai, China; [3]Department of Radiology, Jinling Hospital, Affiliated Hospital of Nanjing University Medical School, Nanjing, China

Contributions: (I) Conception and design: YE Zhao, Q Hu, G Lu, S Luo; (II) Administrative support: G Lu, D Jin, S Luo; (III) Provision of study materials or patients: YE Zhao, Q Hu, J Zhu, M Sun; (IV) Collection and assembly of data: YE Zhao, Q Hu, J Zhu, H Zhang; (V) Data analysis and interpretation: YE Zhao, Q Hu, J Chen, H Zhang; (VI) Manuscript writing: All authors; (VII) Final approval of manuscript: All authors.

[#]These authors contributed equally to this work.

Correspondence to: Song Luo, MD. Department of Radiology, Geriatric Hospital of Nanjing Medical University, No. 65, Jiangsu Road, Nanjing 210002, China. Email: hnldls@163.com.

Background: Coronary artery calcium scoring (CACS) is a noninvasive method for quantifying coronary artery calcification plaque burden. Although low-dose chest computed tomography (LD-CT) scans with energy-integrating detector CT can be used for CACS, its clinical utility is constrained by higher mean differences and wider limits of agreement. In contrast, photon-counting CT offers significantly enhanced image quality compared to energy-integrating detector CT, making it a more promising tool for accurate CACS. This study investigated the difference in CACS obtained from LD-CT using photon-counting detector CT as compared to standard CACS CT (CAC-CT).

Methods: This prospective study included 105 patients (mean age 64.6±11.5 years) who underwent both CAC-CT and LD-CT scans on the same day using photon-counting detector CT. CAC-CT served as a reference standard. Ten groups generated by LD-CT were reconstructed using different strength levels of quantum iterative reconstruction (QIR; 0–4) and slice thickness (3 and 1.5 mm), with the $LD_{3mm\text{-}QIR0}$ to $LD_{1.5\ mm\text{-}QIR4}$ groups being designated. The accuracy of CACS detection via LD-CT was evaluated using the intraclass correlation coefficient (ICC; >0.9: excellent) with two-way mixed effects and absolute agreement, Bland-Altman analysis, and weighted kappa (excellent: >0.8) being used for risk categorization agreement. The Wilcoxon signed-rank test was used to compare the radiation doses between CAC-CT and LD-CT. P<0.05 was considered to indicate statistical significance.

Results: Coronary artery calcium was detected in 77 (73.3%) patients via CAC-CT. Each LD-CT group demonstrated high sensitivity (96.1–100%) and specificity (100%) in detecting coronary artery calcium, with all cases detected in the $LD_{1.5\ mm\text{-}QIR0}$ and $LD_{1.5\ mm\text{-}QIR1}$ groups. Excellent agreement in CACS was observed between the LD-CT groups and the CAC-CT group (ICC: 0.983–0.993). $LD_{1.5\ mm\text{-}QIR2}$ showed the narrowest limits of agreement, while $LD_{1.5\ mm\text{-}QIR1}$ showed the lowest mean bias. The volume CT dose index was reduced by approximately 56.5% with LD-CT as compared to with CAC-CT (1.0 *vs.* 2.3 mGy; P<0.001).

Conclusions: The LD-CT scan derived from photon-counting detector CT demonstrated excellent agreement with the standard CACS scan in terms of CACS and significantly reduced radiation dose. The

^ ORCID: 0000-0003-4797-4120.

reconstruction protocol using a 1.5-mm slice thickness with QIR level 1 improved coronary artery calcium detection, quantification, and risk categorization.

Keywords: Computed tomography (CT); photon-counting detector; calcium score; low-dose CT; iterative reconstruction

Submitted Jun 20, 2024. Accepted for publication Feb 19, 2025. Published online Mar 25, 2025.
doi: 10.21037/qims-24-1244
View this article at: https://dx.doi.org/10.21037/qims-24-1244

Introduction

Coronary atherosclerotic heart disease is a major contributor to cardiovascular morbidity and mortality globally (1). Vascular calcification is a common pathological feature of atherosclerosis. The coronary artery calcium scoring (CACS) is a useful, noninvasive tool for diagnosing coronary heart disease. It is also a valuable prognostic marker that can facilitate risk stratification and treatment decision-making in patients with coronary heart disease (2). Traditionally, determining the CACS using a dedicated electrocardiograph (ECG)-triggered computed tomography (CT) scanning protocol, known as standard CACS CT (CAC-CT) scan, has served as a reference standard for noninvasive detection and quantification of coronary artery calcification. Recent studies (3,4) have demonstrated that low-dose (LD) chest CT (LD-CT) scans with a non-ECG trigger can also be used to evaluate CACS. Although there is good agreement regarding CACS between LD-CT images and standard ECG-triggered CT from energy-integrating detector CT, studies have shown a relatively high mean difference and wide limits of agreement, limiting the clinical application of this approach (5,6).

In contrast to conventional energy-integrating detector CT, which combines the electrical signal of multiple X-ray photons into a single intensity value, photon-counting detector CT (PCD-CT) individually measures the number and energy of X-ray photons, enhancing tissue contrast, stabilizing Hounsfield units (HU), suppressing electronic noise, and reducing noise-aliasing artifacts (7,8). These advancements have enabled the use of PCD-CT as an innovative technique, opening new possibilities for low-dose imaging, particularly for screening. A previous study demonstrated that the CACS obtained with PCD-CT is more accurate than is energy-integrating detector CT when the CAC-CT scan is used and that LD lung cancer screening with PCD-CT provides better image quality while using a considerably lower radiation dose than energy-integrating detector-CT scans (9). If LD lung cancer screening with PCD-CT can accurately quantify CACS, it may serve as a comprehensive tool for both lung cancer screening and cardiovascular risk assessment with reduced radiation dose exposure as compared to energy-integrating detector CT scans.

No studies on the accuracy CACS using photon-counting CT chest scans have been conducted. Additionally, the Agatston score, a commonly used method for CACS calculation, is greatly affected by acquisition parameters (such as tube voltage) and reconstruction parameters (such as slice thickness and kernel) (10). The aim of this study was thus to identify the differences in CACS obtained through LD-CT scan using PCD-CT with tin filtration (Sn 100 kVp) under various reconstruction parameters in comparison to those of standard CACS. We present this article in accordance with the STARD reporting checklist (available at https://qims.amegroups.com/article/view/10.21037/qims-24-1244/rc).

Methods

Study design and patients

This prospective study was conducted in accordance with the Declaration of Helsinki (as revised in 2013) and was approved by the ethics board of the Geriatric Hospital of Nanjing Medical University (No. 044-1). Informed consent was obtained from all participants prior to enrollment. A total of 112 patients who required lung cancer screening and cardiovascular risk assessment were recruited consecutively at the Geriatric Hospital of Nanjing Medical University between December 2023 and March 2024. The LD-CT and CAC-CT were performed on the same day. Patients with a history of coronary artery bypass grafting, stenting surgery, or cardiac metal implantation were excluded. The

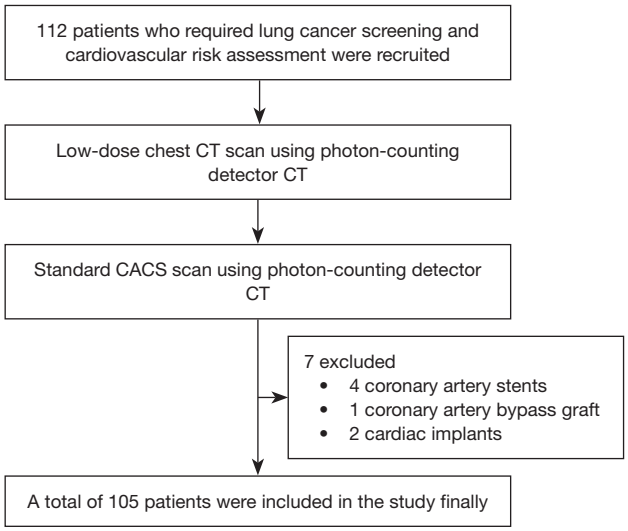

Figure 1 The flowchart of the study. CACS, coronary artery calcium scoring; CT, computed tomography.

Table 1 The acquisition and reconstruction parameters for the CAC-CT and LD-CT scans

Parameter	LD-CT	CAC-CT
Acquisition parameter		
ECG triggered	Non-ECG triggered	ECG triggered
Acquisition mode	Spiral	Prospective sequential
Tube voltage (kVp)	Sn 100	120
Collimation (mm)	144×0.4	144×0.4
Image quality level	19	19
Pitch	3.2	NA
Rotation time (s)	0.25	0.25
Scan range	Lung apex to lung base	Tracheal carina to heart apex
Reconstruction parameter		
Monoenergetic level (keV)	70	70
Iterative reconstruction	QIR 0–4	QIR 2
Kernel	Qr36	Qr36
Slice thickness (mm)	3, 1.5	3
Increment (mm)	1.5, 1.0	1.5
Matrix size	512×512	512×512

CAC-CT, standard coronary artery calcium scoring computed tomography; ECG, electrocardiograph; LD-CT, low-dose chest computed tomography; QIR, quantum iterative reconstruction.

study flowchart can be found in *Figure 1*.

Data acquisition and reconstruction parameters

Scans were acquired using a first-generation clinical dual-source PCD-CT system (NAEOTOM Alpha with syngo. CT VA50; Siemens Healthineers, Erlangen, Germany). Initially, an LD-CT was performed, followed by a CAC-CT. The LD-CT scan covered the entire lungs from the apex to base, while the CAC-CT scan covered the entire heart from the tracheal carina to the heart apex. All CT acquisitions were performed in the craniocaudal direction. We did not use the circulatory agonists such as beta blockers during in the study.

The scan and reconstruction parameters are presented in *Table 1*. Axial images from the CAC-CT were used as reference images. For CAC-CT, the reconstruction parameters for CACS images were based on the manufacturer's recommended protocol and involved monoenergetic reconstruction at 70 keV, kernel at Qr36, and quantum iterative reconstruction (QIR) at the intermediate level (QIR 2) (11). For LD-CT, the reconstruction parameters were performed using different combinations of two different slice thicknesses/increments (3/1.5 mm and 1.5/1 mm) (5) and five QIR levels (QIR 0–4). A total of 11 groups were generated, including CAC-CT (as the reference group), $LD_{3\ mm\text{-}QIR0}$ to $LD_{3\ mm\text{-}QIR4}$, and $LD_{1.5\ mm\text{-}QIR0}$ to $LD_{1.5mm\text{-}QIR4}$. The CACS from 10 LD-CT groups were assessed to identify the closest match with the CAC-CT group. All 11 groups of images were performed under soft tissue window settings (width 400 HU; level 40 HU).

CAC quantification and risk categorization

One experienced researcher with over 10 years of experience in cardiovascular radiology (Y.E.Z.) analyzed the presence and score of CAC in the 11 groups. Calcification was defined as a lesion area of ≥1.03 mm^2 with an attenuation value of >130 HU (12). The CACS was determined using the Agatston method (12). For CAC detection, a CACS >0 was considered indicative of the presence of CAC, and a CACS score of 0 indicated the absence of CAC. Discordant cases (in which CAC was present on only one scan) were analyzed together with another expert reader with over 15 years of experience in cardiovascular radiology (S.L.) to confirm the discrepancy in CAC presence. CAC was automatically quantified using software (CT CaScoring,

syngo.via VB60, Siemens Healthineers) (12). The reader then decided whether it was truly a coronary calcification and included or excluded it. Agatston scores were recorded with one decimal place. Risk categories based on the Agatston score were defined as follows: very low risk (0), low risk (>0–10), moderate risk (>10–100), moderately high risk (>100–400), and severe risk (>400) (13).

Objective image quality assessment

To select images of sufficient quality for quantifying coronary artery calcium (CAC), we measured the noise and signal-to-noise ratio (SNR) of the 11 image groups. Quantitative image assessment was performed by a single reader on a dedicated workstation (syngo.via VB60B, Siemens Healthineers), placing a region of interest (approximately 1.0 cm^2 in size) in the ascending aortic root. CT attenuation and standard deviation, which served as noise, were documented. The SNR was calculated by dividing the CT attenuation by the noise.

Radiation dose

To compare the radiation doses of the two different scan methods, the volume CT dose index (CTDIvol) and dose-length product (DLP) values documented were recorded. The effective dose (ED) in millisieverts (mSv) was calculated using the following formulas (5) and two conversion factors (14):

- $ED_{CAC\text{-}CT}$ (mSv) = DLP (mGy × cm) × 0.026 (mSv × mGy^{-1} × cm^{-1}).
- $ED_{LD\text{-}CT}$ (mSv) = DLP (mGy × cm) × 0.014 (mSv × mGy^{-1} × cm^{-1}).

Statistical analysis

Statistical analyses were performed using SPSS software version 24 (IBM Corporation, Armonk, NY, USA). The normality of the distribution of continuous variables was assessed using the Kolmogorov-Smirnov test. Normally distributed continuous variables are presented as the mean ± standard deviation, and nonnormally distributed continuous variables are presented as the median with interquartile range. Categorical variables are presented as the frequency (percentage). P<0.05 was considered to indicate statistical significance.

The sensitivity, specificity, and accuracy of the LD-CT groups for detecting CAC were calculated using the CAC-CT group as a reference. Differences in CACS between the LD-CT groups and CAC-CT were compared using one-way analysis of variance or the Friedman test with Bonferroni correction, depending on the distribution. The Pearson or Spearman correlation coefficient was used to assess the correlation between CACS derived from LD-CT and CAC-CT acquisitions, depending on the distribution. Agreement was assessed using Bland-Altman analysis (mean bias, upper and lower limits of agreement) and the intraclass correlation coefficient (ICC) with two-way mixed effects and absolute agreement. ICC values <0.5, between 0.5 and 0.75, between 0.75 and 0.9, and >0.90, indicated poor, moderate, good, and excellent reliability, respectively (15). The limits of agreement were determined using Bland-Altman analysis. The agreement in risk categorization between the LD-CT groups and CAC-CT was evaluated using weighted kappa (from 0 to 1.00, with 0.81–1.00 indicating excellent agreement) (15). The image quality (in terms of noise and SNR) was compared using one-way analysis of variance or the Friedman test with Bonferroni correction, depending on the distribution. The difference in the radiation dose between LD-CT and CAC-CT was assessed using the paired *t*-test or Wilcoxon signed-rank test based on the distribution.

Results

Patient characteristics

According to the inclusion criteria, a total of 112 patients were enrolled, all of whom successfully underwent LD-CT scans and CAC-CT scans on the same day. Subsequently, based on the exclusion criteria, 7 patients were excluded, 4 due to coronary artery stents, 1 due to a coronary artery bypass graft, and 2 due to cardiac implants. Finally, a total of 105 patients were included in the study. The baseline characteristics of study participants are summarized in *Table 2*.

CAC score quantification and risk categorization

CAC was detected in 73.3% (77/105) of patients in the CAC-CT group. With the CAC-CT group serving as the reference, for all the LD-CT groups, there was high sensitivity, specificity, and accuracy in CAC detection with no false-positive results in any of the LD-CT groups. CAC was accurately detected in all patients in the $LD_{1.5mm\text{-}QIR0}$ and $LD_{1.5mm\text{-}QIR1}$ groups. The detailed results of CAC detection for the 10 LD-CT groups are listed in *Table 3*.

The CACS was not normally distributed (Figure S1);

Table 2 Baseline characteristics of the study participants

Variables	Value (n=105)
Age (years)	64.6±11.5
Male	75 (71.4)
Height (cm)	165.2±25.5
Weight (kg)	74.1±13
BMI (kg/m^2)	26.7±3.5
Heart rate (bpm)	74.6±15
Hypertension	42 (40.0)
Diabetes	36 (34.3)
Dyslipidemia	22 (21)
Tobacco abuse	12 (11.4)
CAD family history	18 (17.1)
Total Agatston score*	117.4 (34.4, 392.1)

Values are expressed as mean ± standard deviation, median (interquartile range), or n (%). *, obtained from standard coronary artery calcium scoring scan (12). BMI, body mass index; CAD, coronary artery disease.

Table 3 Coronary artery calcium detection performance in the 10 groups of LD-CT compared to that of CAC-CT (n=105)

Group	SE (%)	SP (%)	Accuracy (%)	Misdiagnosis (n)
$LD_{3mm\text{-}QIR0}$	98.7	100	99.5	1
$LD_{3mm\text{-}QIR1}$	97.4	100	98.1	2
$LD_{3mm\text{-}QIR2}$	97.4	100	98.1	2
$LD_{3mm\text{-}QIR3}$	96.1	100	97.1	3
$LD_{3mm\text{-}QIR4}$	96.1	100	97.1	3
$LD_{1.5mm\text{-}QIR0}$	100	100	100	0
$LD_{1.5mm\text{-}QIR1}$	100	100	100	0
$LD_{1.5mm\text{-}QIR2}$	98.7	100	99.5	1
$LD_{1.5mm\text{-}QIR3}$	98.7	100	99.5	1
$LD_{1.5mm\text{-}QIR4}$	97.4	100	98.1	2

CAC-CT, standard coronary artery calcium scoring computed tomography; LD, low dose; LD-CT, low-dose chest computed tomography; n, are the number of patients; QIR, quantum iterative reconstruction; SE, sensitivity; SP, specificity.

therefore, the differences in CACS between the LD-CT groups and CAC-CT were compared using the Friedman test and Wilcoxon signed-rank test with Bonferroni correction used for pairwise group comparisons. The Friedman test revealed a significant difference in the distribution of CACS between the groups (P<0.001). The CACS of the $LD_{1.5mm\text{-}QIR1}$, $LD_{1.5mm\text{-}QIR2}$, and $LD_{1.5mm\text{-}QIR3}$ groups (median CACS of 130.7, 130.1, and 129.3, respectively) did not significantly differ to that of the CAC-CT group (median 117.4; P>0.05). The Spearman correlation coefficients and ICCs between the LD-CT groups and CAC-CT group ranged from 0.987 to 0.99 (all P<0.001) and from 0.983 to 0.993 (all P<0.001), respectively. The absolute mean bias calculated using the Bland-Altman method ranged from 1.5 to 30. Among the groups, $LD_{1.5mm\text{-}QIR1}$ showed the lowest absolute mean bias. An illustrative example is provided in *Figure 2*. The limits of agreement, also calculated using the Bland-Altman method, ranged from 173.3 to 224.8. Notably, among the LD-CT groups, $LD_{1.5mm\text{-}QIR2}$ and $LD_{1.5mm\text{-}QIR1}$ exhibited a narrower limit of agreement (173.3 and 174, respectively). The detailed results are presented in *Table 4*.

The weighted kappa values indicating the agreement in CACS risk categorization between the LD-CT groups and the CAC-CT group ranged from 0.84 to 0.9, with the $LD_{1.5mm\text{-}QIR3}$ group showing the highest level of agreement. The reclassification rate for the LD-CT groups ranged from 7.6% to 12.4%. Underestimated severity classifications in LD-CT groups ranged from 2.8% to 9.5%, while overestimated severity classifications in LD-CT groups ranged from 1% to 9.5%. The detailed results are presented in *Table 5*.

Objective image quality and radiation dose

The noise, SNR, CTDIvol, and ED did not follow a normal distribution. There were significant differences in noise and SNR between the 11 groups (*Table 6*). $LD_{3mm\text{-}QIR3}$, $LD_{3mm\text{-}QIR4}$, and $LD_{1.5mm\text{-}QIR4}$ exhibited superior objective image quality as compared to the other reconstruction groups, showing similar objective image quality to that of CAC-CT (all P values >0.05). Except for that in the $LD_{1.5mm\text{-}QIR0}$ group, the noise level in all the groups was <23 HU, meeting the image noise requirement for assessing CACS (16). The detailed results are presented in *Table 6*.

In terms of radiation dose, the CTDIvol and ED of LD-CT scan were significantly lower than those of CAC-CT (*Table 7*).

Discussion

Our principal finding is that in comparison to CAC-CT,

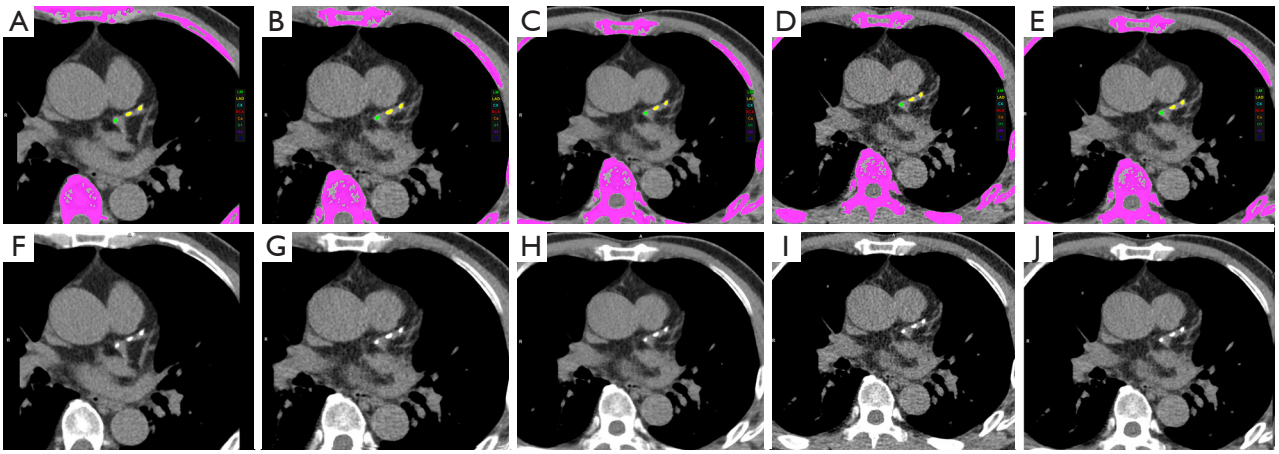

Figure 2 Comparison of CACS between the LD-CT and standard CAC-CT in a 68-year-old male with a heart rate of 67 bpm. (A,F) The CAC-CT group (reference group), (CACS: 266.7). (B,G) The $LD_{3mm\text{-}QIR1}$ group (CACS: 242.7). (C,H) The $LD_{3mm\text{-}QIR3}$ group (CACS: 241.5). (D,I) The $LD_{1.5mm\text{-}QIR1}$ group (CACS: 266.8). (E,J) The $LD_{1.5mm\text{-}QIR3}$ group (CACS: 258.5). CAC-CT, standard coronary artery calcium scoring computed tomography; CACS, coronary artery calcium scoring; CT, computed tomography; LD, low dose; LD-CT, low-dose chest computed tomography; QIR, quantum iterative reconstruction.

Table 4 Comparison of Agatston scores between LD-CT and CAC-CT acquisitions (n=77)

Group	Agatston score	P*	r*	ICC*	Bias*	LOA*
CAC-CT	117.4 (34.4, 392.1)	–	–	–	–	–
$LD_{3mm\text{-}QIR0}$	107 (32, 377.6)	0.001	0.99	0.988 (0.978, 0.993)	−21.2	−124.8/82.5
$LD_{3mm\text{-}QIR1}$	105.4 (28.9, 376.4)	<0.001	0.991	0.986 (0.971, 0.992)	−26.3	−136.6/84.1
$LD_{3mm\text{-}QIR2}$	99.9 (30, 370.6)	<0.001	0.988	0.985 (0.968, 0.992)	−27.8	−140.2/84.6
$LD_{3mm\text{-}QIR3}$	101.4 (29.4, 371.9)	<0.001	0.988	0.984 (0.967, 0.992)	−29.6	−145.1/85.9
$LD_{3mm\text{-}QIR4}$	104.6 (29.6, 364)	<0.001	0.988	0.983 (0.965, 0.991)	−30	−146.9/86.9
$LD_{1.5mm\text{-}QIR0}$	137.2 (48.5, 409.1)	<0.001	0.988	0.992 (0.986, 0.995)	15.6	−73.8/105.1
$LD_{1.5mm\text{-}QIR1}$	130.7 (43.8, 389.2)	0.5	0.989	0.993 (0.989, 0.996)	1.5	−85.5/88.5
$LD_{1.5mm\text{-}QIR2}$	130.1 (41.3, 385.3)	1.0	0.99	0.993 (0.989, 0.996)	−4.2	−90.9/82.4
$LD_{1.5mm\text{-}QIR3}$	129.3 (37.3, 377.9)	0.3	0.988	0.984 (0.967, 0.992)	−8.4	−96.1/79.3
$LD_{1.5mm\text{-}QIR4}$	129.7 (33.8, 376.9)	0.002	0.987	0.983 (0.965, 0.991)	−13.5	−106.9/79.8

Values are expressed as median (interquartile range). *, comparison of Agatston score derived from LD-CT and CAC-CT acquisitions. CAC-CT, standard coronary artery calcium scoring computed tomography; ICC, intraclass correlation coefficient; LD, low dose; LD-CT, low-dose chest computed tomography; LOA, limit of agreement; QIR, quantum iterative reconstruction.

LD-CT demonstrated high accuracy in CAC detection and excellent agreement in CAC quantification and risk categorization under a reconstruction parameter of 1.5-mm slice thickness and a QIR level of 1. Additionally, LD-CT scans exhibited a remarkable 56.6% reduction in CTDIvol compared to CAC-CT.

In LD-CT performed with PCD-CT, the reconstruction parameters influence not only the detection of CAC but also the accuracy of quantification and risk categorization of CACS. In CAC detection, a thinner slice thickness (1.5 mm) combined with lower-level iterative algorithms (QIR 0–1) improves the accuracy of CAC detection as compared to other reconstruction parameter combinations. This explains how a thicker slice thickness can lead to the CT

Table 5 Risk categorization based on Agatston score for CAC-CT and LD-CT

Group	CACS risk categorization					Rate (%)	Kappa
	Very low risk	Low risk	Moderate risk	Moderately high risk	Severe risk		
CAC-CT	28	8	27	23	19	–	–
$LD_{3mm\text{-}QIR0}$	29	7	29	23	17	8.6 (7↓, 2↑)	0.889
$LD_{3mm\text{-}QIR1}$	30	7	28	23	17	9.5 (8↓, 2↑)	0.887
$LD_{3mm\text{-}QIR2}$	30	8	29	21	17	10.5 (10↓, 1↑)	0.865
$LD_{3mm\text{-}QIR3}$	31	8	26	23	17	9.5 (9↓, 1↑)	0.877
$LD_{3mm\text{-}QIR4}$	31	8	27	22	17	9.5 (9↓, 1↑)	0.865
$LD_{1.5mm\text{-}QIR0}$	28	5	27	25	20	12.4 (3↓, 10↑)	0.840
$LD_{1.5mm\text{-}QIR1}$	28	6	29	23	19	9.5 (4↓, 6↑)	0.877
$LD_{1.5mm\text{-}QIR2}$	29	5	29	23	19	9.5 (4↓, 6↑)	0.877
$LD_{1.5mm\text{-}QIR3}$	29	6	30	22	18	7.6 (5↓, 3↑)	0.900
$LD_{1.5mm\text{-}QIR4}$	30	5	29	23	18	8.6 (5↓, 4↑)	0.889

Data are expressed as the numbers of patients. ↓, number of underestimated severity classifications; ↑, number of overestimated severity classifications; %, reclassification rate. CAC-CT, standard coronary artery calcium scoring computed tomography; CACS, coronary artery calcium scoring; LD, low dose; LD-CT, low-dose chest computed tomography; QIR, quantum iterative reconstruction.

Table 6 Comparison of image quality between CAC-CT and LD-CT

Group	CT attenuation (HU)	Noise (HU)	P	SNR	P
CAC-CT	47 (44, 50)	13 (11, 15)		3.7 (3.1, 4.1)	
$LD_{3mm\text{-}QIR0}$	44 (40, 49)	23 (21, 26)	<0.001	2.0 (1.7, 2.1)	<0.001
$LD_{3mm\text{-}QIR1}$	44 (40, 49)	18.5 (17, 20)	<0.001	2.5 (2.1, 2.7)	<0.001
$LD_{3mm\text{-}QIR2}$	44 (40, 49)	16 (15, 18)	<0.001	2.8 (2.4, 3.1)	0.01
$LD_{3mm\text{-}QIR3}$	44 (40, 49)	14 (12, 15)	1.0	3.1 (2.8, 3.7)	1.0
$LD_{3mm\text{-}QIR4}$	44 (41, 49)	11 (10, 13)	0.558	3.9 (3.3, 4.6)	1.0
$LD_{1.5mm\text{-}QIR0}$	44 (39, 49)	31.5 (28, 34)	<0.001	1.5 (1.3, 1.6)	<0.001
$LD_{1.5mm\text{-}QIR1}$	44 (40, 49)	22 (20, 26.3)	<0.001	2.0 (1.6, 2.1)	<0.001
$LD_{1.5mm\text{-}QIR2}$	44 (40, 49)	21 (19, 23)	<0.001	2.1 (1.9, 2.4)	<0.001
$LD_{1.5mm\text{-}QIR3}$	44 (40, 49)	17 (16, 19)	<0.001	2.6 (2.3, 2.8)	<0.001
$LD_{1.5mm\text{-}QIR4}$	44 (41, 49)	14 (13, 18)	1.0	3.2 (2.7, 3.6)	1.0

Values are expressed as median (interquartile range). CAC-CT, standard coronary artery calcium scoring computed tomography; HU, Hounsfield unit; LD, low dose; LD-CT, low-dose chest computed tomography; QIR, quantum iterative reconstruction; SNR, signal-to-noise ratio.

value for calcifications dropping below 130 HU due to the partial volume effect, resulting in missed diagnoses (12). Additionally, higher levels of iterative reconstruction may misidentify small calcification foci as noise, leading to their subsequent removal. In the CACS quantification and risk categorization, under a 1.5-mm slice thickness, low and moderate QIR levels produced a similar CACS to that of CAC-CT, while the highest QIR level significantly underestimated the CACS. This underestimation is likely due to the misclassification of small calcifications as being noise at the highest QIR level, resulting in their removal. Therefore, appropriate settings must be selected to

Table 7 Comparison of radiation dose between CAC-CT and LD-CT

Variable	CAC-CT	LD-CT	P
CTDIvol (mGy)	2.3 (1.9, 2.7)	1.0 (0.9, 1.1)	<0.001
ED (mSv)	0.7 (0.6, 0.9)	0.5 (0.4, 0.5)	<0.001

Values are expressed as median (interquartile range). CAC-CT, standard coronary artery calcium scoring computed tomography; CTDIvol, CT dose-index volume; ED, effective dose; LD-CT, low-dose chest computed tomography.

balance the advantages and drawbacks of each examination and achieve accurate quantification of CACS at the lowest possible radiation dose. The relevant guidelines recommended maintaining the noise level below 23 HU for the evaluation of CACS (15). In our study, except for the $LD_{1.5mm\text{-}QIR0}$ group, all the groups had noise levels below 23 HU, meeting the requirements for CACS assessment. Therefore, considering image noise and balancing the accuracy of coronary artery calcification detection, quantification, and risk stratification, we recommend a 1.5-mm slice thickness and a QIR level of 1 as the optimal parameters for evaluating CAC via LD-CT.

Despite there being good agreement in CACS between LD-CT and CAC-CT under the energy-integrating detector CT, previous studies have reported relatively high mean differences and wide limits of agreement, potentially limiting clinical application. In our study, the correlation and agreement of $LD_{1.5mm\text{-}QIR1}$ were similar to those produced by Sn 100 kVp chest CT reported by Xiao *et al.* (r=0.993; ICC =0.99) (5) and Vingiani *et al.* (r=0.99; ICC not mentioned) (17). Moreover, $LD_{1.5mm\text{-}QIR1}$ did not significantly differ from CAC-CT but showed smaller mean bias and narrower limits of agreement as compared to those of previous studies (6). These findings suggest that LD-CT using PCD-CT has excellent agreement with standard CACS scan in terms of CACS and reduces the mean bias between the two methods. This improvement can be attributed to enhanced tissue contrast, no electronic noise, and reduced noise-aliasing artifacts afforded by the PCD-CT system. Additionally, the $LD_{1.5mm\text{-}QIR1}$ group showed similar agreement in risk categorization (weighted kappa =0.9) to that reported by Xiao *et al.* (5), who used a third-generation dual-source CT scanner with different CACS categories and a higher weighted kappa of 0.54 than that of Liu *et al.* (3), who employed a third-generation dual-source CT scanner at the Sn 100 kVp in the chest scans with the same CACS categories.

In terms of radiation dose, we observed a significant reduction in CTDIvol with LD-CT as compared with CAC-CT. The CTDIvol values in our study were notably lower than those reported in a previous study on low-dose CT lung cancer screening (18), aligning with the American College of Radiology's recommendations for low-dose lung screening (9). Regarding the anatomical region-specific weighting factors, the ED for LD-CT was significantly reduced in our study, which is in line with findings from previous studies using PCD-CT at Sn 100 kVp for LD lung screening (19).

Certain limitations to our study should be acknowledged. First, we employed a single-center design, and prospective, multicenter studies are required to obtain more robust evidence. Second, our results are limited to PCD-CT technology and may not be applicable to other CT systems. Third, we did not evaluate the impact of body mass index (BMI) on CACS derived from LD-CT. A previous study demonstrated the impact of BMI on calcium quantification (20); thus, appropriate patient BMI cutoff values need to be determined in future studies.

Conclusions

LD-CT scan with PCD-CT can accurately quantify CACS, and reconstruction protocols using a 1.5-mm slice thickness and QIR level 1 can improve the detection and quantification of CAC, as well as cardiovascular risk categorization. This approach could serve as serve as a comprehensive tool for both lung cancer screening and cardiovascular risk assessment with reduced radiation dose as compared to standard CAC-CT.

Acknowledgments

None.

Footnote

Reporting Checklist: The authors have completed the STARD reporting checklist. Available at https://qims.amegroups.com/article/view/10.21037/qims-24-1244/rc

Funding: This study was supported by Jiangsu Provincial Health Care Project (No. BJ23017).

Conflicts of Interest: All authors have completed the ICMJE uniform disclosure form (available at https://qims.amegroups.com/article/view/10.21037/qims-24-1244/coif).

J.C. is an employee of Siemens Healthineers. The other authors have no conflicts of interest to declare.

Ethical Statement: The authors are accountable for all aspects of the work in ensuring that questions related to the accuracy or integrity of any part of the work are appropriately investigated and resolved. This study was conducted in accordance with the Declaration of Helsinki (as revised in 2013) and was approved by the ethics board of Geriatric Hospital of Nanjing Medical University (No. 044-1). Informed consent was obtained from all participants.

References

1. Global burden of 288 causes of death and life expectancy decomposition in 204 countries and territories and 811 subnational locations, 1990-2021: a systematic analysis for the Global Burden of Disease Study 2021. Lancet 2024;403:2100-32.
2. Onnis C, Virmani R, Kawai K, Nardi V, Lerman A, Cademartiri F, Scicolone R, Boi A, Congiu T, Faa G, Libby P, Saba L. Coronary Artery Calcification: Current Concepts and Clinical Implications. Circulation 2024;149:251-66.
3. Liu Y, Chen X, Liu X, Yu H, Zhou L, Gao X, Li Q, Su S, Wang L, Zhai J. Accuracy of non-gated low-dose non-contrast chest CT with tin filtration for coronary artery calcium scoring. Eur J Radiol Open 2022;9:100396.
4. Groen RA, Jukema JW, van Dijkman PRM, Bax JJ, Lamb HJ, Antoni ML, de Graaf MA. The Clear Value of Coronary Artery Calcification Evaluation on Non-Gated Chest Computed Tomography for Cardiac Risk Stratification. Cardiol Ther 2024;13:69-87.
5. Xiao H, Wang X, Yang P, Wang L, Xu J. Coronary artery calcium scoring assessment in ultra-low-dose chest computed tomography. Clin Imaging 2024;106:110045.
6. Osborne-Grinter M, Ali A, Williams MC. Prevalence and clinical implications of coronary artery calcium scoring on non-gated thoracic computed tomography: a systematic review and meta-analysis. Eur Radiol 2024;34:4459-74.
7. Xing Q, Cai A, Zheng Z, Li L, Yan B. Enhancing photon-counting computed tomography reconstruction via subspace dictionary learning and spatial sparsity regularization. Quant Imaging Med Surg 2025;15:581-607.
8. Dunning CAS, Marsh JF Jr, Winfree T, Rajendran K, Leng S, Levin DL, Johnson TF, Fletcher JG, McCollough CH, Yu L. Accuracy of Nodule Volume and Airway Wall Thickness Measurement Using Low-Dose Chest CT on a Photon-Counting Detector CT Scanner. Invest Radiol 2023;58:283-92.
9. Inoue A, Johnson TF, Walkoff LA, Levin DL, Hartman TE, Burke KA, Rajendran K, Yu L, McCollough CH, Fletcher JG. Lung Cancer Screening Using Clinical Photon-Counting Detector Computed Tomography and Energy-Integrating-Detector Computed Tomography: A Prospective Patient Study. J Comput Assist Tomogr 2023;47:229-35.
10. Christensen JL, Sharma E, Gorvitovskaia AY, Watts JP Jr, Assali M, Neverson J, Wu WC, Choudhary G, Morrison AR. Impact of Slice Thickness on the Predictive Value of Lung Cancer Screening Computed Tomography in the Evaluation of Coronary Artery Calcification. J Am Heart Assoc 2019;8:e010110.
11. Eberhard M, Mergen V, Higashigaito K, Allmendinger T, Manka R, Flohr T, Schmidt B, Euler A, Alkadhi H. Coronary Calcium Scoring with First Generation Dual-Source Photon-Counting CT-First Evidence from Phantom and In-Vivo Scans. Diagnostics (Basel) 2021;11:1708.
12. Gupta A, Bera K, Kikano E, Pierce JD, Gan J, Rajdev M, Ciancibello LM, Gupta A, Rajagopalan S, Gilkeson RC. Coronary Artery Calcium Scoring: Current Status and Future Directions. Radiographics 2022;42:947-67.
13. Kim SM, Chung MJ, Lee KS, Choe YH, Yi CA, Choe BK. Coronary calcium screening using low-dose lung cancer screening: effectiveness of MDCT with retrospective reconstruction. AJR Am J Roentgenol 2008;190:917-22.
14. Trattner S, Halliburton S, Thompson CM, Xu Y, Chelliah A, Jambawalikar SR, Peng B, Peters MR, Jacobs JE, Ghesani M, Jang JJ, Al-Khalidi H, Einstein AJ. Cardiac-Specific Conversion Factors to Estimate Radiation Effective Dose From Dose-Length Product in Computed Tomography. JACC Cardiovasc Imaging 2018;11:64-74.
15. Jirapatnakul A, Yip R, Myers KJ, Cai S, Henschke CI, Yankelevitz D. Assessing the impact of nodule features and software algorithm on pulmonary nodule measurement

uncertainty for nodules sized 20 mm or less. Quant Imaging Med Surg 2024;14:5057-71.
16. Voros S, Rivera JJ, Berman DS, Blankstein R, Budoff MJ, Cury RC, Desai MY, Dey D, Halliburton SS, Hecht HS, Nasir K, Santos RD, Shapiro MD, Taylor AJ, Valeti US, Young PM, Weissman G; Society for Atherosclerosis Imaging and Prevention Tomographic Imaging and Prevention Councils; Society of Cardiovascular Computed Tomography. Guideline for minimizing radiation exposure during acquisition of coronary artery calcium scans with the use of multidetector computed tomography: a report by the Society for Atherosclerosis Imaging and Prevention Tomographic Imaging and Prevention Councils in collaboration with the Society of Cardiovascular Computed Tomography. J Cardiovasc Comput Tomogr 2011;5:75-83.
17. Vingiani V, Abadia AF, Schoepf UJ, Fischer AM, Varga-Szemes A, Sahbaee P, Allmendinger T, Tesche C, Griffith LP, Marano R, Martin SS. Low-kV coronary artery calcium scoring with tin filtration using a kV-independent reconstruction algorithm. J Cardiovasc Comput Tomogr 2020;14:246-50.
18. Demb J, Chu P, Yu S, Whitebird R, Solberg L, Miglioretti DL, Smith-Bindman R. Analysis of Computed Tomography Radiation Doses Used for Lung Cancer Screening Scans. JAMA Intern Med 2019;179:1650-7.
19. Graafen D, Emrich T, Halfmann MC, Mildenberger P, Düber C, Yang Y, Othman AE, O' Doherty J, Müller L, Kloeckner R. Dose Reduction and Image Quality in Photon-counting Detector High-resolution Computed Tomography of the Chest: Routine Clinical Data. J Thorac Imaging 2022;37:315-22.
20. Tesche C, De Cecco CN, Vliegenthart R, Albrecht MH, Varga-Szemes A, Duguay TM, Ebersberger U, Bayer RR 2nd, Canstein C, Schmidt B, Allmendinger T, Litwin SE, Morris PB, Flohr TG, Hoffmann E, Schoepf UJ. Accuracy and Radiation Dose Reduction Using Low-Voltage Computed Tomography Coronary Artery Calcium Scoring With Tin Filtration. Am J Cardiol 2017;119:675-80.

Cite this article as: Zhao YE, Hu Q, Zhu J, Zhang H, Chen J, Sun M, Jin D, Lu G, Luo S. Evaluation of low-dose chest scans for coronary artery calcium scoring using photon-counting computed tomography with different slice thicknesses and iterative reconstruction levels. Quant Imaging Med Surg 2025;15(4):3565-3574. doi: 10.21037/qims-24-1244

